Journal of Solid State Chemistry 182 (2009) 331–338

Contents lists available at ScienceDirect

Journal of Solid State Chemistry

journal homepage: www.elsevier.com/locate/jssc

Crystal structure and magnetic properties of the solid-solution phase $Ca_3Co_{2-v}Mn_vO_6$

C.H. Hervoches [a], H. Okamoto [b], A. Kjekshus [b,*], H. Fjellvåg [b], B.C. Hauback [a]

[a] Institute for Energy Technology, N-2007 Kjeller, Norway
[b] Centre for Materials Science and Nanotechnology, Department of Chemistry, University of Oslo, P.O. Box 1033 Blindern, N-0315 Oslo, Norway

ARTICLE INFO

Article history:
Received 18 June 2008
Received in revised form
7 October 2008
Accepted 11 October 2008
Available online 12 November 2008

Keywords:
Manganese substituted $Ca_3Co_2O_6$
Crystal structure
Magnetic structure
Magnetic phase diagram

ABSTRACT

The homogeneity range of the $Ca_3Co_{2-v}Mn_vO_6$ solid-solution phase covers the entire composition interval from $v = 0$ to 1. A systematic powder X-ray and neutron diffraction, magnetic susceptibility, and magnetization study has been carried out to investigate effects of the Mn-for-Co substitution on structural and magnetic properties. The Mn substitution concerns primarily only the octahedral Co1 site of the $Ca_3Co1Co2O_6$ crystal structure, whereas the trigonal-prismatic Co2 site structurally is left essentially unaffected. The $Ca_3Co_{2-v}Mn_vO_6$ crystal structure belongs to space group $R3c$ with unit-cell dimensions (in hexagonal setting) $9.084 \leqslant a \leqslant 9.134$ Å and $10.448 \leqslant c \leqslant 10.583$ Å. A cut through the magnetic phase diagram at 10 K shows a ferrimagnetic domain for $0 \leqslant v < \sim 0.3$ and an antiferromagnetic domain for $\sim 0.50 < v < \sim 1$. The magnetic ordering temperatures are quite low ($< \sim 25/18$ K), and even so further magnetic transitions appear to take place at still lower temperature. The legitimity and reliability of the different indicators used to establish the magnetic transitions, their individual accuracy, and mutual consistency are briefly discussed. Variable parameters of the crystal and magnetic structures of $Ca_3Co1_{1-v}Mn_vCo2O_6$ are determined and their variation with v is briefly discussed in relation to chemical bonding. The magnetic structure in the ferrimagnetic region is essentially the same as that of the pristine $v = 0$ phase, but since the moments at the Co2 site decrease and those at the (Co1,Mn) site increase with increasing v; characteristic traits of ferrimagnetism in magnetic susceptibility and magnetization gradually disappear. The magnetic arrangement in the antiferromagnetic region is characterized by differently sized moments at the (Co1,Mn) and Co2 sites, moments at adjacent sites in each of these sublattices being oppositely oriented along [001].

1. Introduction

$Ca_3Co_2O_6$ and derivatives thereof are exciting materials with several interesting properties which have been subjected to numerous theoretical and experimental studies over the last decade or so. The valence, spin, and orbital states of the Co atoms are issues which have been frequently addressed in this connection. The particular attention on valence was certainly triggered by an article [1] in which some of the present authors were careless to proclaim that the two crystallographically non-equivalent Co atoms carry different oxidation states. The actual message which we wanted to convey (and which was rooted in our results) is that, owing to the mixed character of the bonding in $Ca_3Co_2O_6$, the valences may be parted into ionic and covalent portions which differ for the octahedral and trigonal-prismatic Co sites. In retrospect we realize that such stretching of the valence concept is incompatible with the IUPAC-definition of oxidation state. We therefore like to use this opportunity to assert that we also support the assignment of the formal oxidation state 3+ to both crystallographic Co atoms. Consensus about the valence issue should accordingly be established in the involved parts of the scientific community. The benefit from our carelessness with inorganic chemical nomenclature is a tremendous amount of high quality experimental and theoretical papers on various properties of exotic $Ca_3Co_2O_6$ which have appeared in the last few years (see, e.g., Refs. [2–12] and references therein).

The present authors have earlier studied substitutional solid-solution phases of $Ca_3Co_2O_6$ with Y [13], La–Lu [13] and Sc [14] where it was found that Sc almost exclusively substitutes for the trigonal-prismatic (t) co-ordinated $Co2^t$ constituent, whereas the Y and La–Lu solutes equally exclusively prefer the Ca site. We have in our studies hitherto not experienced replacement at the octahedrally (o) co-ordinated $Co1^o$ site, but this has been reported for the solutes Cr [15] (with notable low solubility), Mn [16–18], Rh [2,11,19–23], and Ir [11,19,20].

The present contribution concerns the $Ca_3Co_{2-v}Mn_vO_6$ phase, which appears to exhibit a somewhat remarkable phase stability; existence at the verge compositions $v = 0$ and 1 with a miscibility

* Corresponding author. Fax: +47 22 85 54 41.
E-mail address: arne.kjekshus@kjemi.uio.no (A. Kjekshus).

0022-4596/$ - see front matter © 2008 Elsevier Inc. All rights reserved.
doi:10.1016/j.jssc.2008.10.016

gap [16] at around $v = 0.5$. Magnetic property data have been interpreted [16] as evidence for Mn^{4+} and Co^{4+} as formal oxidation states for the residents at the Co1^o site. This interpretation, however, is not in conformity with the now commonly accepted view that Co at both sites takes the formal oxidation state 3+ in $Ca_3Co_2O_6$ (*vide supra*). The magnetic properties of $Ca_3Co_{2-v}Mn_vO_6$ have, more generally, hitherto not been fully clarified, in particular with regard to co-operative magnetic state(s).

In March this year, when the first version of the present manuscript was about to be submitted, a paper by Choi et al. [18] came to our attention. This very interesting contribution deals with magnetism-driven ferroelectricity, a fundamental topic which belongs to the more central and challenging problems in current days materials science, solid-state physics, and solid-state chemistry. Choi et al. make use of $Ca_3Co_{2-v}Mn_vO_6$ (mostly with $v = 0.96$) to experimentally test the theoretically predicted ferroelectricity for an Ising-chain magnet. Most of the paper is focused on ferroelectric aspects, and only a brief description of the co-operative magnetic structure at $v = 0.96$ is included (a composition not studies by us). The actual overlap with the present paper is very small and the two studies may therefore properly be regarded as complementary.

The $Ca_3Co_{2-v}Mn_vO_6$ phase takes the same K_4CdCl_6-type crystal structure as the pristine phase [24,25], *viz.* an atomic arrangement with a distinct quasi-one-dimensional character, comprising $(Co_{2-v}Mn_vO_6)_\infty$ columns of alternating face-sharing (Co1,Mn)O_6 octahedra and Co2O_6 trigonal prisms. The columns are separated by Ca^{2+} cations which counterbalance the more evenly distributed negative charges in the oxygen framework on the outside of the columns.

2. Experimental section

A series of single-phase samples of $Ca_3Co_{2-v}Mn_vO_6$ was prepared from weighed amounts of $CaCO_3$ (Merck, p.a.), $Co(CH_3COO)_2 \cdot 4H_2O$ (Fluka, mass fraction >99.0%), and $Mn(NO_3)_2 \cdot 4H_2O$ (Alfa, mass fraction >99.98%) according to the citrate-gel method [citric acid monohydrate, $C_3H_4(OH)(COOH)_3 \cdot H_2O$ (Sigma–Aldrich, mass fraction >99.0–102.0%)]. The precise content of Co in $Co(CH_3COO)_2 \cdot 4H_2O$ and Mn in $Mn(NO_3)_2 \cdot 4H_2O$ was determined by means of thermogravimetric analysis. The desired amount of $CaCO_3$ was first dissolved in an aqueous solution of citric acid. When the dissolution was completed, excess amount of the citric acid was introduced and subsequently aqueous solutions of $Co(CH_3COO)_2 \cdot 4H_2O$ and $Mn(NO_3)_2 \cdot 4H_2O$ were added under stirring. This mixture was then heated on a hot plate at ~170 °C until a clear, pink-colored, glassy gel had appeared. The gel was dehydrated at 150 °C (overnight) into a solid xerogel that was milled and incinerated at 450 °C in air for a few hours in order to remove carbonaceous species. The thus obtained amorphous precursor was then ground in an agate mortar, pressed into pellets, and repeatedly fired at 1000 °C. These heat treatments lasted for 48 h and in between the samples were subjected to re-homogenization.

All samples were checked for phase purity and subsequently characterized at room temperature by powder X-ray diffraction (PXD) using a Bruker AXS D5000 diffractometer with monochromatic Cu$K\alpha_1$ radiation ($\lambda = 1.540598$ Å) and position sensitive detectors. Lattice parameters were determined by the so-called Le Bail method.

Powder neutron diffraction (PND) data were collected with the high-resolution PND PUS [26] at the JEEP II reactor, Kjeller, Norway. Cylindrical vanadium sample holders were used. Monochromatic neutrons with wavelength $\lambda = 1.5554$ or 1.5562 Å (1.825 Å for a duplicate sample of $Ca_3Co_2O_6$) were obtained from a Ge(511) focusing monochromator. The detector unit consists of two banks of seven position-sensitive ^{3}He detectors, each covering 20° in 2θ. Intensity data were collected from $2\theta = 10$–130° in steps of $\Delta(2\theta) = 0.05°$. Temperatures between 8 and 298 K were measured and controlled by means of a silicon diode. Structure determination and profile refinement were performed using the Rietveld refinement program Fullprof [27]. The background was described by linear interpolation between selected points. One scale factor, two unit-cell dimensions, four pseudo-Voigt profile parameters, and the zero point, were accounted for together with four positional parameters, four isotropic displacement factors (two of which being constrained), four occupancy factors (two of which being constrained), and two components for the magnetic moments. The regions 46.00–46.90, 76.90–77.60, and 115.90–117.20° were excluded due to faint reflections originating from the displex cooling system.

Magnetic properties were investigated using a superconducting-quantum-interference-device (SQUID) magnetometer (MPMS, Quantum Design). Dc-magnetization measurements were carried out according to the dc-extraction method in both field-cooled (FC) and zero-field-cooled (ZFC) modes at $H = 100$ Oe and $5 \leqslant T \leqslant 300$ K. The field dependence of magnetization (up to 5 T) was investigated at 10 K.

3. Results and discussion

3.1. Solid solubility and structural features

The homogeneity range of the $Ca_3Co_{2-v}Mn_vO_6$ phase covers the composition range $0 \leqslant v \leqslant 1$. Phase-pure samples were obtained for all compositions within this range, and the unit-cell dimensions increase virtually linearly with increasing v (Fig. 1).

The incomplete solid-solubility around $v = 0.5$ introduced by Bazuev et al. [16] must accordingly reflect insufficient homogenizing of their samples. Bazuev et al. used the solid-state-reaction technique for their syntheses, whereas the present study adopted the citrate-gel technique. Our experience with the solid-state-reaction technique for synthesis of non-melting multi-component compounds is that this approach usually requires that the entire procedure with milling and mixing, pellet pressing, and annealing may have to be repeated numerous times in order to ensure proper equilibrium. The citrate-gel technique on the

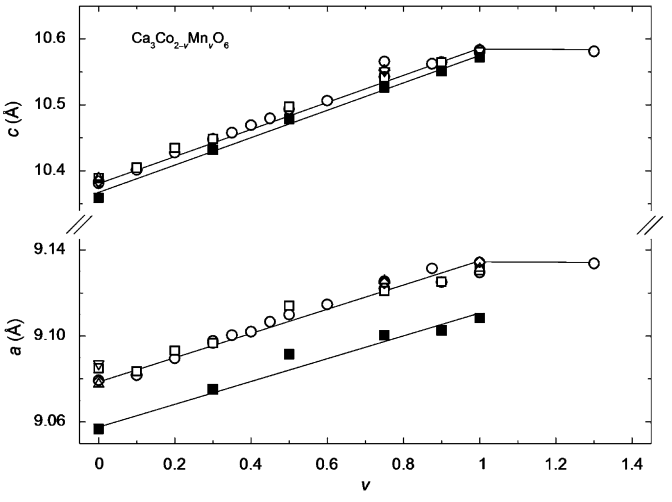

Fig. 1. Variation in unit-cell dimensions with Mn content (v) for $Ca_3Co_{2-v}Mn_vO_6$. Points marked ○ and □ refer, respectively, to present PXD and PND data at 298 K and ■ to PND data at 8/10 K. The points marked △, ▽, and ◇ at 298 K are quoted from Refs. [16,17,24].

other hand, has the advantage that the components are mixed on the atomic level already before the heat treatment commences. All evidences gathered for the present samples confirm that the equilibrium state has been reached.

The Mn-rich phase limit of $Ca_3Co_{2-v}Mn_vO_6$ is estimated to go at $v = 1.00 \pm 0.04$, making use of the disappearing-phase criterion and the constancy of unit-cell dimensions in neighbouring two-phase fields (see Fig. 1). A substitution extent of $v = 1$ corresponds to complete filling of one of the two Co sites by Mn, *viz.* gives a stoichiometric compound with the formula Ca_3CoMnO_6. Rietveld refinement of the room-temperature PND data according to the structure specification for $Ca_3Co1_{1-v}Mn_vCo2O_6$ advanced in Refs. [16,17] indeed confirmed the suppositions. However, the refined values for the occupancies of Mn on the $Co1^o$ (6*b* position) and $Co2^t$ (6*a* position) sites (see Table 1) fair enough show a certain distribution of Mn between the two sites. The thus inferred disorder could indicate that the samples had not come to complete equilibrium. However, we rather believe that these findings reflect a computational imcompatibility, which arises because the refinement program did not allow simultaneous constraints on the total amount of Mn available for distribution on the Co1 and Co2 sites (*viz. v*) and complete filling of both sites (*viz.* 100% occupancy by Co and Mn jointly). These requirements can be satisfied separately but not together, and for the present computations we chose to ensure complete filling of all sites. The slight deviations between chemical formulae and refined occupancies (Table 1) have likely come from the implied simplification of the refinement model.

Unit-cell dimensions and atomic co-ordinates, obtained by profile refinements of PND data collected at 298 and 8/10 K, are listed in Table 1. The generally low values for the reliability factors and standard deviations ascertain that the assumed structure model ($Ca_3Co1_{1-v}Mn_vCo2O_6$ in space group $R3c$, site by site directly derived from the pristine compound) as well as the fitting procedure are adequate. Significant amounts of oxygen defects were not detected in the refinements, and the postulated oxygen content of six per formula unit were accordingly accepted without separate analysis.

Table 1
Unit cell dimensions[a], atomic co-ordinates[a], site occupancies[a], and magnetic moments[b] as obtained by Rietveld refinements of powder neutron diffraction data for $Ca_3Co_{2-v}Mn_vO_6$; data referring to 298 and 8/10 K are printed in roman and italics, respectively.

Composition		$v = 0$	v = 0.30	$v = 0.50$	$v = 0.75$	v = 0.90	$v = 1$
a (Å)		9.0850(3)	9.0967(1)	9.1208(1)	9.1208(1)	9.1251(1)	9.1304(1)
		9.0567(3)	*9.0751(1)*	*9.0901(1)*	*9.1002(1)*	*9.1026(1)*	*9.1082(1)*
c (Å)		10.3888(3)	10.4481(2)	10.4967(2)	10.5410(2)	10.5643(1)	10.5795(1)
		10.3589(5)	*10.4310(2)*	*10.4785(2)*	*10.5262(1)*	*10.5500(1)*	*10.5720(1)*
Ca	x	0.3692(2)	0.3671(3)	0.3664(3)	0.3645(3)	0.3638(2)	0.3631(2)
		0.3706(5)	*0.3674(3)*	*0.3665(2)*	*0.3649(2)*	*0.3640(2)*	*0.3630(2)*
	B (Å^2)	0.30(8)	0.53(5)	0.56(5)	0.46(4)	0.1(4)	0.32(4)
		1.3(1)	*0.24(5)*	*0.32(4)*	*0.20(3)*	*0.12(3)*	*0.14(3)*
$(Co1,Mn)^o$	B (Å^2)[c]	0.1(1)	0.8(3)	0.9(2)	0.25(1)	0.35(9)	0.44(9)
		0.9(1)	*0.3(1)*	*0.9(1)*	*0.10(6)*	*0.01(5)*	*0.22(4)*
	Occ.[d]	n.a.	0.743(1)	0.534(1)	0.210(2)	0.072(1)	–0.054(1)
		n.a.	*0.743(1)*	*0.534(1)*	*0.210(2)*	*0.072(1)*	*–0.054(1)*
	$\mu_{Co1,Mn}$ (μ_B)	*0.1(2)*	*0.62(7)*	*0.87(4)*	*1.22(3)*	*1.34(2)*	*0.66(5)*
$Co2^t$	B (Å^2)[c]	0.1(1)	0.8(3)	0.9(2)	0.25(1)	0.35(9)	0.44(9)
		1.3(1)	*0.3(1)*	*0.9(1)*	*0.10(6)*	*0.01(5)*	*0.22(4)*
	Occ.[d]	1	1.000(1)	1.000(1)	0.978(1)	1.000(1)	0.984(1)
		1	*1.000(1)*	*1.000(1)*	*0.978(1)*	*1.000(1)*	*0.984(1)*
	μ_{Co2} (μ_B)	*2.93(4)*	*1.38(6)*	*0.2(14)*	*0.0(2)*	*0.2(1)*	*0.1(1)*
O	x	0.1766(1)	0.1766(2)	0.1767(2)	0.1777(2)	0.1778(1)	0.1780(1)
		0.1758(3)	*0.1775(2)*	*0.1778(1)*	*0.1782(1)*	*0.1780(1)*	*0.1781(1)*
	y	0.0244(1)	0.0243(2)	0.0240(2)	0.0240(2)	0.0240(1)	0.0241(1)
		0.0209(5)	*0.0247(2)*	*0.0241(2)*	*0.0242(1)*	*0.0242(1)*	*0.0238(1)*
	z	0.1138(1)	0.1116(1)	0.1101(1)	0.1086(1)	0.1085(1)	0.1079(8)
		0.1141(2)	*0.1118(1)*	*0.1104(1)*	*0.1088(1)*	*0.1085(1)*	*0.1087(1)*
	B (Å^2)	0.28(7)	0.91(4)	0.92(4)	0.67(3)	0.31(3)	0.30(3)
		1.4(1)	*0.54(4)*	*0.50(2)*	*0.36(2)*	*0.12(1)*	*0.08(2)*
	Occ.	1	1	1	1	1	1
		1	*1*	*1*	*1*	*1*	*1*
R_{wp}		4.04	7.79	7.48	6.97	5.39	5.44
		5.90	*7.45*	*6.34*	*5.71*	*4.98*	*5.37*
R_p		3.12	5.90	5.64	5.48	4.27	4.27
		4.52	*5.87*	*5.00*	*4.53*	*3.92*	*4.15*
χ^2		0.624	1.93	2.92	1.54	0.993	1.31
		1.01	*1.81*	*1.27*	*1.25*	*1.02*	*1.59*
$R_{mag.}$		*17.3*	*22.5*	*28.9*	*12.2*	*15.3*	*15.1*

[a] According to space group $R3c$ (hexagonal setting) with Ca in 18*c* (*x*,0,1/4) etc, $(Co1,Mn)^o$ in 6*b* (0,0,0) etc, $Co2^t$ in 6*a* (0,0,1/4) etc, and O in 36*f* (*x*,*y*,*z*) etc.
[b] Magnetic structure described in space group $P3$ (see text).
[c] The isotropic displacement parameters for $(Co1,Mn)^o$ and $Co2^t$ sites were constrained.
[d] The occupancies of the $(Co1,Mn)^o$ and $Co2^t$ sites were constrained (complete filling), but no constraint was imposed on the distribution of the *v* Mn atoms between the sites.

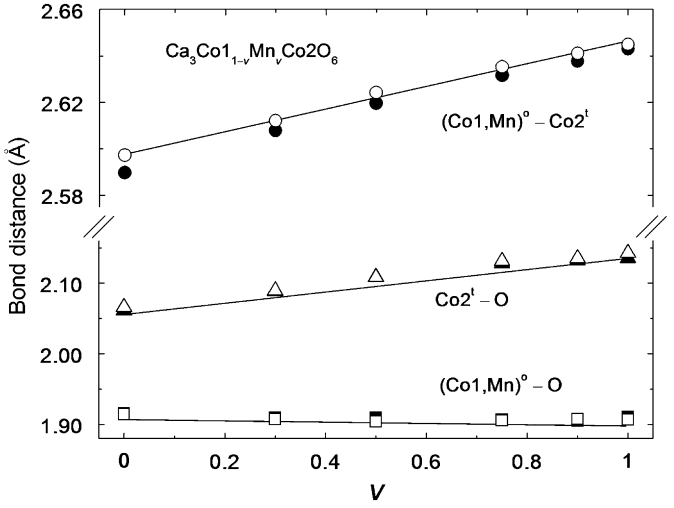

Fig. 2. Variation in the bonding interatomic distances (Co1,Mn)^{o}–O (o = octahedral co-ordination), Co2^{t}–O (t = trigonal-prismatic co-ordination), and (Co1,Mn)^{o}–Co2^{t} with Mn content (v) of $Ca_3Co_{2-v}Mn_vO_6$. Open and filled symbols refer to 298 and 8/10 K, respectively.

The variable atomic co-ordinates are subject to small systematic changes as function of degree of substitution (v) and temperature (T) (see Table 1). The variation in bonding interatomic distances with v and T (Fig. 2) is largely imposed by the variations in the unit-cell dimensions. The compositional variation of these distances is a key to insight into the chemical consequences of the Mn-for-Co1 substitution. Whereas the (Co1,Mn)^{o}–O distance only has increased by 0.4% up to the phase boundary, the Co2^{t}–O and (Co1,Mn)^{o}–Co2^{t} distances have expanded by 3.7 and 1.9%, respectively. The overall picture corresponds to our findings for the closely related solid-solution phases $Ca_{3-v}Y_vCo1Co2O_6$ [13] and $Co_3Co1Co2_{1-v}Sc_vO_6$ [14]. However, on the more detailed level, the relation of course differs in the three cases. In $Co_3Co1Co2_{1-v}Sc_vO_6$ the Co2^{t} site is directly affected by the Sc-for-Co2 substitution and the increased (Co2,Sc)^{t}–O and Co1^{o}–(Co2,Sc)^{t} distances are occasioned by the larger size of Sc. In $Ca_{3-v}Y_vCo1Co2O_6$ any effect of the Y-for-Ca substitution on the Co sublattices must be indirect. On the basis of structural and magnetic properties for the latter phase, it was concluded [13] that a electron-transfer process takes place between the Co2^{t} and (Ca,Y) sublattices, effectively lowering the formal oxidation state of v Co2 atoms per formula unit from 3+ to 2+. (The ionic terminology is used for its convenience in charge accounting while the chemical bonding in the phases under consideration definitely has a distinct covalent woof [1].)

The $Ca_3Co1_{1-v}Mn_vCo2O_6$ phase is in a somewhat analogous situation to $Ca_{3-v}Y_vCo1Co2O_6$ in that the substitution, that takes place on one sublattice, manifests itself as an effect on another sublattice. The simplest ionic interpretation of the formula $Ca_3Co1_{1-v}Mn_vCo2O_6$ would be that Mn enters as 3+. However, since the 3+ state of Mn appears to the less stable than the 2+ and 4+ states, we subscribe to the suggestion in Refs. [16,18] that Mn occurs in the 4+ state in $Ca_3Co1_{1-v}Mn_vCo2O_6$. A corresponding amount of Co2^{t} must accordingly be converted from 3+ to 2+ to maintain charge balance. (Note that the thus inferred charge sequence …Co^{2+}–Mn^{4+}–Co^{2+}… is in accordance with Pauling's [28] electrostatic valence rule, which states that the electrostatic charges in an ionic crystal are balanced locally around every ion as evenly as possible.) We believe that the essential features of the variation in the bond distances with the Mn content (Fig. 2) can be explained qualitatively on the basis of this simple model. An obstacle for a more quantitative accounting for the findings is the lack of access to radii for the involve ions resolved according to oxidation and spin states.

3.2. Magnetic susceptibility and magnetization

The temperature dependence of the magnetic susceptibility of $Ca_3Co_{2-v}Mn_vO_6$ (Fig. 3) shows deviation (magnitude and character depend on v) from Curie–Weiss law behaviour below some 100 K. Fig. 4 shows the composition dependences of the paramagnetic moment (μ_p), corresponding spin-only quantum number (S_p), and Weiss constant (θ) [as obtained by least squares fitting of experimental data for the interval 100–300 K to $\chi^{-1}_{mol} = C^{-1}_{mol}(T-\theta)$].

The present findings for the paramagnetic state of $Ca_3Co_{2-v}Mn_vO_6$ agree with those reported in Refs. [16,17,25] when probable distinctions between samples prepared by different

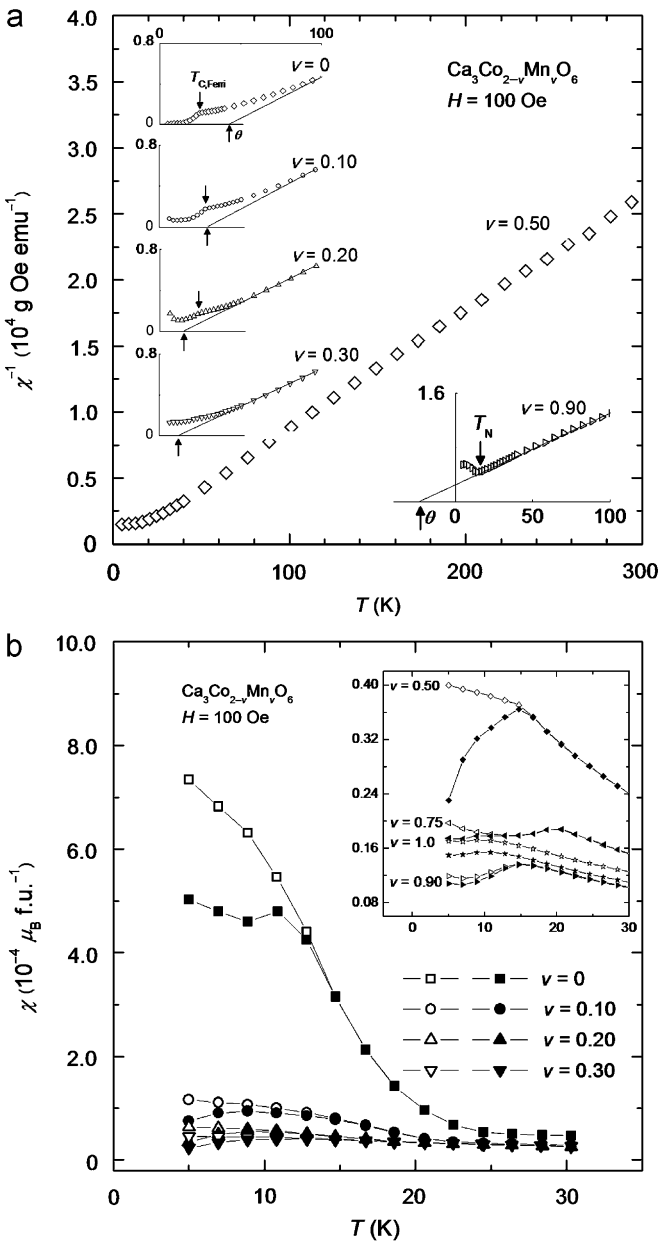

Fig. 3. Temperature variation of magnetic susceptibility ($H = 100$ Oe) for selected compositions of $Ca_3Co_{2-v}Mn_vO_6$ [Mn content (v) is marked on the illustrations]. Arrow shows location of transition temperature according to signature in magnetic susceptibility data: (a) $\chi^{-1}(T)$ plots and (b) $\chi(T)$ plots. Open and filled symbol refer to field-cooled (FC) and zero-field-cooled (ZFC) measurements, respectively.

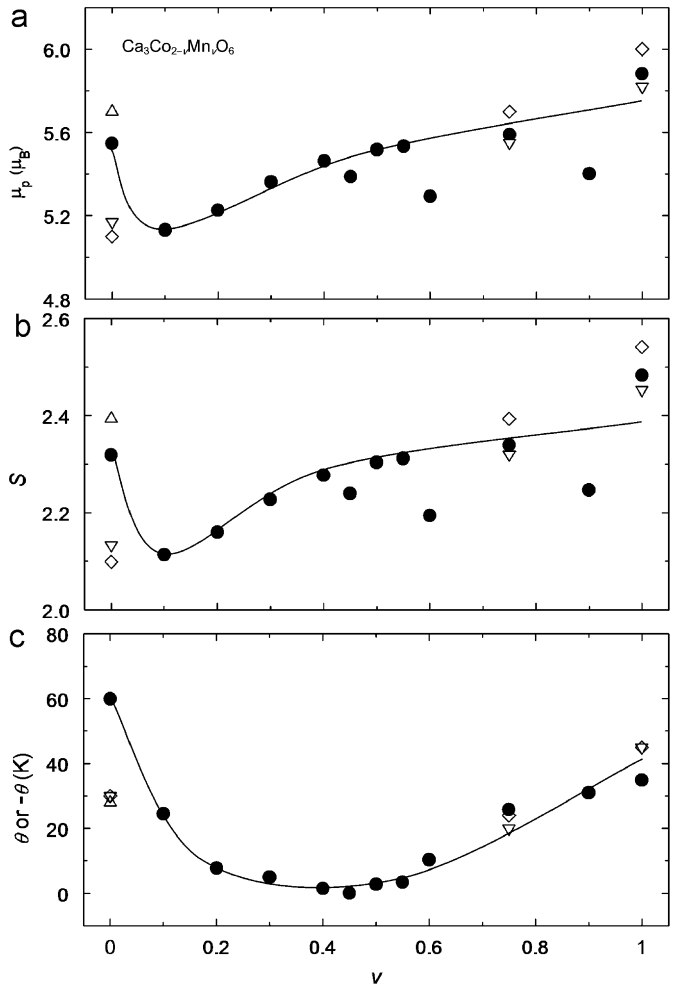

Fig. 4. Variation of average: (a) paramagnetic moment (μ_p), (b) corresponding spin-quantum number [assuming that the spin-only approximation is valid; S from $\mu_p = 2\sqrt{S(S+1)}$] per transition metal atom, and (c) Weiss constant (θ; $|\theta|$ for $0.5 < v \leqslant 1$), with Mn content (v) of $Ca_3Co_{2-v}Mn_vO_6$. Points marked △, ▽, and ◇ are quoted from Refs. [16,17,25].

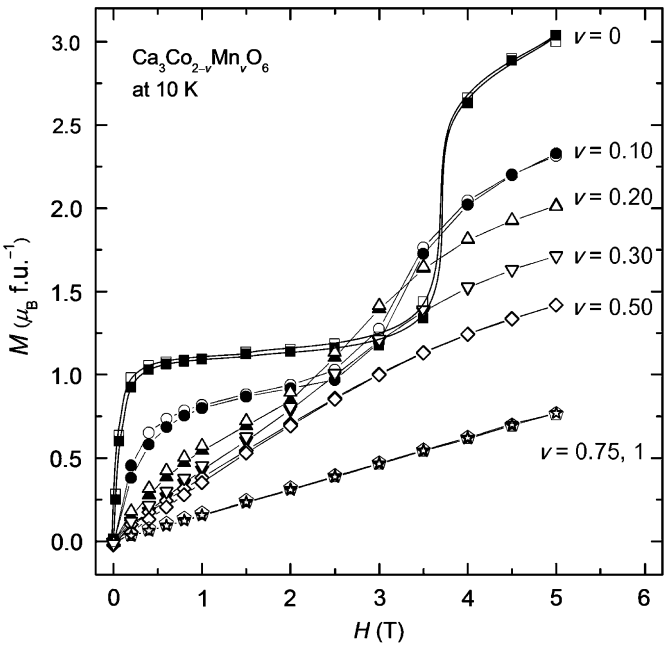

Fig. 5. Magnetization (M) vs. external magnetic field (H) at 10 K. Measurements recorded on increasing and decreasing H are marked with filled and open symbols, respectively. Mn content (v) is marked on the illustration.

methods are taken into account. The smooth variation of μ_p and θ (Fig. 4; $|\theta|$ for $0.5 < v \leqslant 1$) indeed confirms that the present $Ca_3Co_{2-v}Mn_vO_6$ samples are mutually consistent. Already the fact that θ apparently changes continuously from positive at $v = 0$, through $\theta = 0$ K at $v \approx 0.5$ to negative at $v = 1$ suggests that the co-operative state converts from ferri- (Ferri) to antiferromagnetic (AF) around $v = 0.5$ (see Section 3.4).

The $\chi^{-1}(T)$ curve shows positive departure (Fig. 3a) from the linear Curie–Weiss law relationship already around 100 K. This feature has also been observed in earlier studies of $Ca_3Co_2O_6$ and related compounds, and is taken as indicative of formation of an AF-type spin-glass (sg) state. At temperatures closer to $T = |\theta|$ the shape of $\chi^{-1}(T)$ changes appearance. On going from $v = 0$ to 0.30 (see Fig. 3a) the characteristic cusp in $\chi^{-1}(T)$ for $v = 0$ at ~25 K gradually disappears and the overall profile becomes more and more featureless. For $\sim 0.50 < v \leqslant 1$, on the other hand, $\chi^{-1}(T)$ curves go through minima at correspondingly low temperatures. Bifurcation of ZFC and FC branches of $\chi(T)$ are also observed in the same temperature range (Fig. 3b).

The magnetization vs. applied magnetic field at 10 K (Fig. 5; for complementary $M(H)$ data for samples with $v = 0$, 0.25, and 1 at other temperatures see Refs. [16,17]) also gradually changes in character on going from $v = 0$ to 1. The $M(H)$ relationship for $v = 0$ has two distinct plateaux, the first being reached already at quite low fields. This is a macroscopic manifestation of the Ferri state, *viz.* alignment of the initially randomly arranged moments in the studied polycrystalline ensemble of particles. A second plateau, which reaches saturation beyond 5 T, corresponds to conversion of the Ferri state into a field-induced ferromagnetic state. Already at an Mn content of $v = 0.10$, the plateaux have become somewhat smeared out, and for $v = 0.30$, they would hardly have been recognized without the guidance from the gradual changes in the characteristics. The increasing smearing of $M(H)$ as well as $\chi^{-1}(T)$ profiles with increasing v from 0 to 0.30 reflects the actual distribution of Mn on the Co sublattices. It is convenient to label the composition interval from $v = 0$ to ~0.30 at low temperature and absence of external fields as a Ferri domain (see Section 3.4). The ultimate F state is apparently reached at increasingly higher fields as the Mn content increases. Only rather minor hysteresis are associated with the 10-K-$M(H)$ characteristics, whereas extended hysteresis region occur at lower temperature [16,17]. From the appearance of the $M(H)$ characteristics (Fig. 5) the borderline between the Ferri and AF states is located somewhere close to $v = 0.5$ at 10 K.

The $M(H)$ characteristics for $v = 0.75$ to 1 (see also Refs. [16–18] and Sections 3.3 and 3.4) belongs to the domain of another co-operative magnetic phase. The $M(H)$ relations for these compositions are strictly linear and there is absolutely no indication of hysteresis (see also Refs. [16,17]). In complete accordance with these findings, an AF state rules at low temperature in the Mn-rich portion of the $Ca_3Co_{2-v}Mn_vO_6$ phase.

3.3. Magnetic structures

The occurrence of additional low-2θ-angle reflections in the 8/10-K-PND diagrams immediately confirms that $Ca_3Co_{2-v}Mn_vO_6$ is subject to co-operative magnetism at low temperature. The magnetic diffraction patterns were indexable on the basis of the chemical (nuclear) unit cell, but most of the magnetic reflections violate the extinction rules of $R3c$. During refinements of the magnetic structures, we used descriptions based on space group

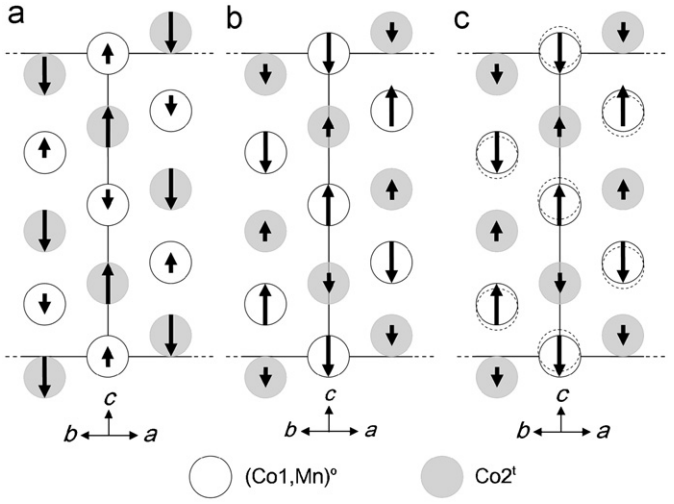

Fig. 6. Schematic representations of the configurations of moments (depicted by unscaled arrows) in the co-operative magnetic states of $Ca_3Co1_{1-v}Mn_vCo2O_6$. The chemical (nuclear) and magnetic unit cells coincide. Only the $(Co1,Mn)^o$ and $Co2^t$ atoms are shown on these cuts from [110] projections of the magnetic structures. (a) The ferrimagnetic (Ferri) structure for $0 \leqslant v < \sim 0.30$. Within each chain the moments at the $Co2^t$ and $(Co1,Mn)^o$ sites are arranged, respectively, ferro- (F) and antiferromagnetically (AF) relative to the moments at the nearest neighbour sites of the same kind. (b) In the AF structure ($\sim 0.5 < v \leqslant 1$) the magnetic sublattices of both $Co2^t$ and $(Co1,Mn)^o$ adopt AF arrangements. (c) The modified AF structure for $v = 0.96$ according to Choi et al. [18]. The distortion of the $(Co1,Mn)^o$ sublattice is indicated by the off-site shifted dotted circles.

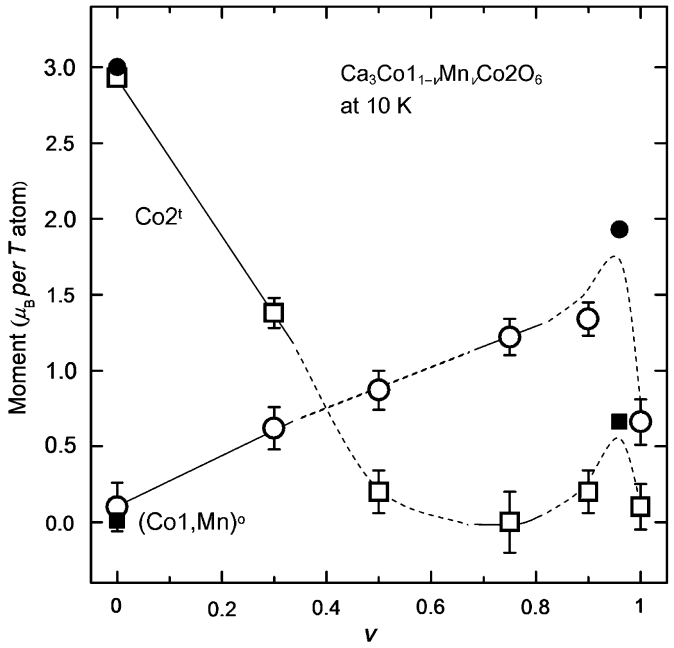

Fig. 7. Evolution of ordered magnetic moments at 8/10 K (in μ_B along [001]; see also Table 1) for $Ca_3Co1_{1-v}Mn_vCo2O_6$. Tentatively realistic estimates for error limits are indicates. PND-based data quoted from Ref. [25] for $v = 0$ (10 K) and from Ref. [18] for $v = 0.96$ (1.4 K) are marked by corresponding filled symbols.

$P3$ (with constrains to comply with $R3c$ for the nuclear unit cell). Our refinement procedure made use of purely magnetic as well as mixed nuclear and magnetic reflections.

The presently derived Ferri structure for the pristine compound (see Fig. 6a) matches that reported in Ref. [25] apart from slightly lower values for the magnetic moments of $Co1^o$ and $Co2^t$ (Table 1). Within the virtually one-dimensional $(CoO_6)_\infty$ chains there occur alternating small moments ($\sim 0.1\ \mu_B$) at the $Co1^o$ sites and larger moments ($\sim 3.0\ \mu_B$) at the $Co2^t$ sites. The moments at $Co1^o$ and $Co2^t$ within each chain are, respectively, AF and F aligned along [001] and the overall Ferri character of $Ca_3Co_2O_6$ is accomplished since one out three moment chains is antiparallel to the other two. This pattern in the arrangement of the magnetic moments is maintained to $v \approx 0.3$. As the amount of Mn increases, the moment on the $(Co1,Mn)^o$ site increases while that on the $Co2^t$ site decreases (Table 1 and Fig. 7). Since the F-arranged magnetic moments at the $Co2^t$ site are large and those in AF-configuration at the $Co1^o$ site is very small, it is quite appropriate to classify the magnetic structure of $Ca_3Co_2O_6$ as Ferri. The magnetic susceptibility and magnetization data for $Ca_3Co_2O_6$ (Section 3.2 and Refs. [16,17]) are in accordance with an assignment to this class. However, the moment at $Co2^t$ decreases and that at $(Co1,Mn)^o$ increases with increasing v (Table 1 and Fig. 7). Hence, the moments at the former site gradually lose their autocratic power on the overall magnetic properties with increasing v (cf. the smearing of the $\chi^{-1}(T)$ and $M(H)$ curves discussed above) the Ferri classification becomes more inappropriate.

In the composition internal $0.50 \leqslant v \leqslant 0.90$ the 8/10-K-PND pattern has changed appearance, magnetic reflections characteristic of the Ferri state have disappeared and a new set of magnetic reflections has turned up. These reflections (see Fig. 4 of Ref. [18] for illustration) were found to originate from an AF arrangement of the magnetic moments which is closely related to that in the neighbouring Ferri structure (cf. parts a and b of Fig. 6). The moments in the sublattices of both $(Co1,Mn)^o$ and $Co2^t$ are aligned AF along [001]. With this model (Fig. 6b), we arrived at acceptable fits to the observed diffraction patterns. Later performed (see Section 1) test calculations according to the composite crystal and magnetic structure model sketched for $Ca_3Co1_{1-v}Mn_vCo2O_6$ with $v = 0.96$ by Choi et al. [18], seemed to give still better fits to our magnetic diffraction patterns for $v = 0.75$ and 0.90. However, the quality of the present data were not considered good enough to justify full-scale least-squares refinements according to the modified model (Fig. 6c) of Choi et al. This differs essentially, only in one feature from that (Fig. 6b) used to derive the crystal and magnetic structure parameters listed in Table 1 for the samples with $v = 0.75$ and 0.90. According to Choi et al. the coupling between the AF and ferroelectricity breaks the inversion symmetry and leads to shift of the magnetic $(Co1,Mn)^o$ atoms along [001], *viz.* to the kind of structural distortion schematically indicated in Fig. 6c. The actural AF arrangement of the moments is of the up-up-down-down type ($\uparrow\uparrow\downarrow\downarrow$).

The moment at the $(Co1,Mn)^o$ site (derived by refinements according to the model in Fig. 6b) continues to increase with increasing Mn content from the Ferri state into the AF state whereas that at the $Co2^t$ site stays low and is burdened with appreciable uncertainty (Table 1 and Fig. 7). The size of the moments at the (Co1,Mn) and Co2 sites [1.34(2) and 0.2(1) μ_B (transition metal atom)$^{-1}$] derived for our $v = 0.90$ sample is significantly smaller than 1.93(3) and 0.66(3) μ_B (transition metal atom)$^{-1}$, respectively, reported for $Ca_3Co_{1.04}Mn_{0.96}O_6$ in Ref. [18]. Apart from emphasizing that the latter data refer to 1.4 K and samples of apparently better crystalline quality we have no explanation to offer for this discrepancy.

The changes in the size of the individual magnetic moments at the $(Co1,Mn)^o$ and $Co2^t$ site over the homogeneity range ($v = 0$ to 1) should, in principle, allow further testing of the supposition (see Section 3.1) that associated with the Mn-for-$Co1^o$ substitution electrons are transferred from Mn to $Co2^t$. However, a simple ionic scheme is difficult to apply for the accounting in this case.

The obstacles are rooted in the fact that the chemical bonding situation in members of the $Ca_3Co_2O_6$ family involves ionic, covalent as well as metallic contributions [1]. There are significant covalent contributions to the bonding between $(Co1,Mn)^o$ and O

as well as between $Co2^t$ and O and the metallic bonding between $(Co1,Mn)^o$ and $Co2^t$ certainly plays a role in the co-operative magnetic ordering. In addition, or rather as consequences of these features, finite magnetic moments are theoretically predicted at the O sites [1]. Moreover, the actual oxygen content appears to have some impact on magnetic moments as well as charge accumulations at certain sites. A further veritable challenge in this connection comes about from the inherent variation in bonding character with v. An additional complication is introduced by the fact that $Ca_3Co_2O_6$ and derivative thereof carries unusually large (giant) orbital moments (see, e.g., Refs. [9,12,22]) which certainly also varies with v. A quantitative testing of the intersite electron transfer concept for $Ca_3Co1_{1-v}Mn_vCo2O_6$ apparently needs quidance from proper first-principles theoretical calculations.

3.4. Tentative magnetic phase diagram

A convenient starting point for a rough sketch of the magnetic phase diagram for the $Ca_3Co_{2-v}Mn_vO_6$ phase is the already established domains of the Ferri and AF states at 8/10 K ($0 \leqslant v < \sim 0.30$ and $\sim 0.50 < v < \sim 1$, respectively).

The traditional direct method for determination of co-operative magnetic transition temperatures is to map the temperature dependence of one (or more) magnetic reflection(s) from the P (sgAF is an alternative which, however, not will be discussed further here) state into the co-operative state and choose as the transition point the highest temperature where the intensity deviates significantly from the background intensity. Fig. 8 shows the findings for $v = 0.30$ ($T_{C,Ferri}$ for the P⇄ Ferri transition) and $v = 0.90$ (T_N for the P⇄ AF transition) according to this approach. The peak intensity vs. temperature plots in Fig. 8 do certainly not follow a Brillouin-type function [29]. [Note that it would theoretically have been more correct to use reduced integrated intensity (I/I_o) vs. reduced temperature ($T/T_{C,Ferri}$ or T/T_N), but already the use of relative peak intensities is misleading, since, e.g., the 100 reflection for $v = 0.30$ is much weaker than the 101 reflection for $v = 0.90$].

Transitions from P to co-operative magnetic states also manifest themselves indirectly in other physical properties. The probably best known and most used of these indicators is the Weiss constant θ from Curie–Weiss law plots which on empirical as well as theoretical basis [29] is formulated as $T_{C,Ferri} \approx \theta$ for $P \rightleftarrows$ Ferri transitions and $T_N \approx -\theta$ for $P \rightleftarrows$ AF transitions. However, there is a considerable number of well documented examples of partly big deviations from these simple "rules". However, we expect that within an estimated accuracy of some 10 K, the "rules" work for the $Ca_3Co1_{1-v}Mn_vCo2O_6$ phase. However, 10 K represents a major woof in relation to $T_{C,Ferri}$ and T_N when one operates in the range 0–30 K.

Closely related to the θ indicator comes the "temperature of deviation from Curie–Weiss law-relationship" indicator (see

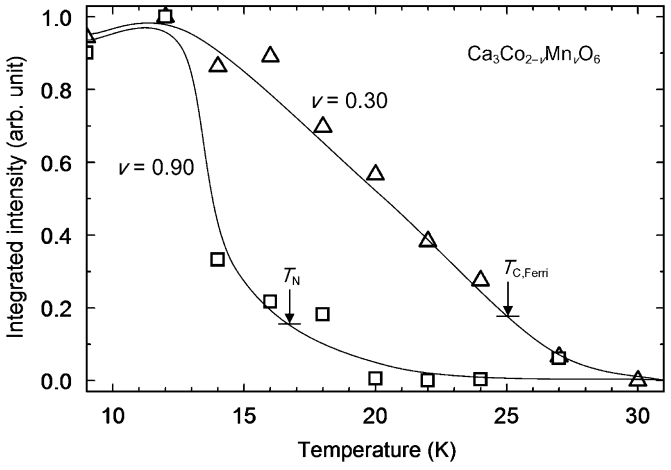

Fig. 8. Selected examples of signature of magnetic transitions in $Ca_3Co_{2-v}Mn_vO_6$ from peak intensity vs. temperature plots for magnetic PND reflections. Assessed location of transition temperature is indicated by arrow.

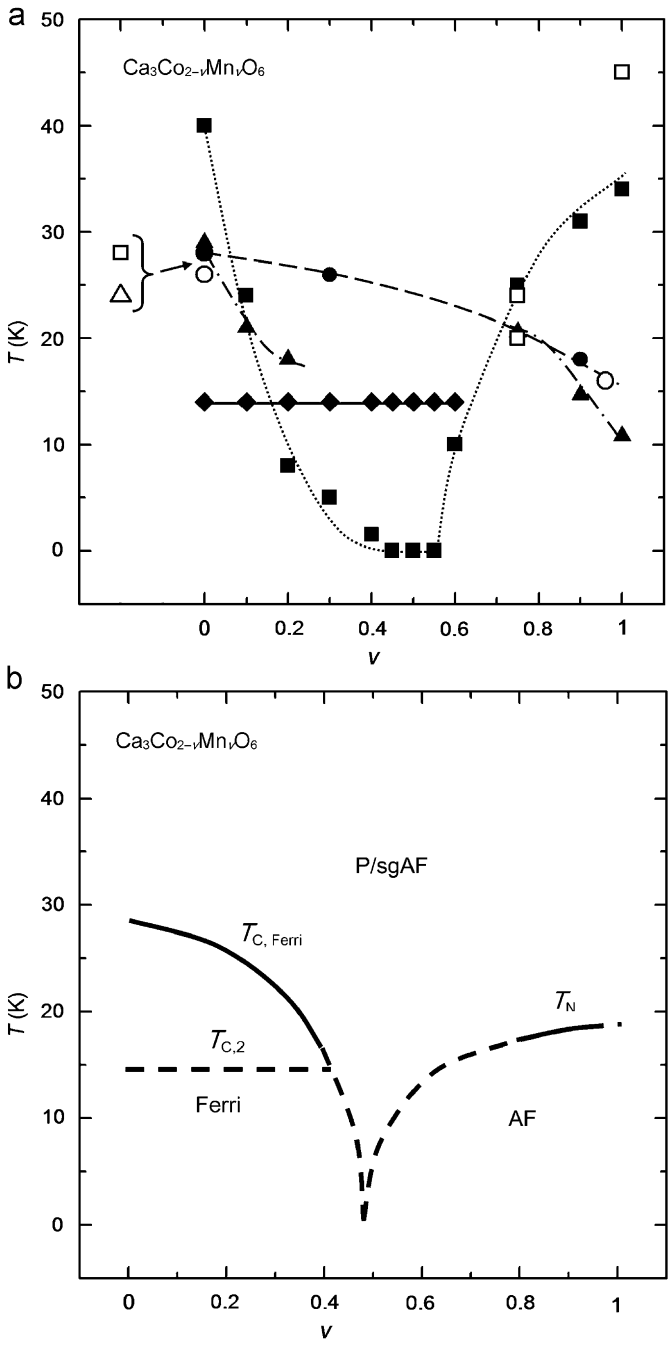

Fig. 9. (a) Magnetic phase-diagram data for $Ca_3Co_{2-v}Mn_vO_6$. The origin of the different pieces of information is indicated by: ● PND data; peak intensity vs. temperature (see Fig. 8), ■ magnetic susceptibility data; θ ($|\theta|$ for negative values), ▲ magnetic susceptibility data; temperature at onset of deviation from Curie–Weiss law (see Fig. 3a), ◆ magnetic susceptibility data; temperature at onset of deviation between FC and ZFC data (see Fig. 3b). Data quoted from Bazuev et al. [16], Rayaprol et al. [17], Choi et al. [18] and Aasland et al. [25] are marked by corresponding open symbols. (b) Tentative magnetic phase diagram abstracted from part a. Magnetic state is designated by P = paramagnetic, sgAF = spin-glass antiferromagnetic, Ferri = ferrimagnetic, and AF = antiferromagnetic.

Fig. 3b). Like θ this indicator has empirical as well as some theoretical backing, but there are also here exceptions. Another drawback with this indicator is that the character of the deviation from linearity of $\chi^{-1}(T)$ appears to depend on the magnetic structure as well as the exchange interactions involved [29]. The $\chi^{-1}(T)$ curve for an ideal ferrimagnet should meet the temperature axis at a vertical tangent. In relation to $\chi^{-1}(T)$ plots for P-to-Ferri-state transitions, departures from ideality are manifested as curve tails which gradually approach $\chi^{-1}=0$ over a temperature range of 20–30 K [see $\chi^{-1}(T)$ for $v=0$ in inset to Fig. 3a]. The occurrence of such curve tails is looked upon as evidences of structural non-ideality in real materials. The temperature for the onset of splitting between of the FC and ZFC magnetic susceptibility (see Fig. 3b) is another marker of change in magnetic state. However, for $Ca_3Co1_{1-v}Mn_vCo2O_6$ it is difficult to ascertain which parts of the Ferri arrangement that is involved. Perhaps it is the ordering of the small moments at the oxygen sites which manifests themselves at the transition; tentatively marked $T_{C,2}$ in Fig. 9b.

Fig. 9a gives a compilation of available information on magnetic transitions in the $Ca_3Co1_{1-v}Mn_vCo2O_6$ phase. If one puts equal weight on all these pieces of information and neglect uncertainties associated with the indicators and their use on the present samples the picture indeed becomes confusing. We therefore decided to draw a tentative magnetic phase diagram mainly on the basis of data provided by PND. The resulting diagram (Fig. 9b) essentially comprises three fields, *viz.* P (or sg AF), Ferri, and AF. An important detail in Fig. 9b which is open for dispute is whether the Ferri and AF fields touch upon each other. If touching actually occurs, then the Ferri and AF regions must be separated by a hysteresis region.

4. Conclusion

The earlier uncertainty about a possible discontinuity in the homogeneity range of the $Ca_3Co1_{1-v}Mn_vCo2O_6$ phase around $v=0.5$ is clarified. The solid-solution phase covers the entire composition interval $0\leqslant v\leqslant 1$ and the overall structural arrangement remains unchanged by the Mn-for-Co substitution at the octahedral Co1 site. The overall magnetic arrangements in the ferri- and antiferromagnetic regions of the $Ca_3Co1_{1-v}Mn_vCo2O_6$ phase are also regarded as coarsely clarified. However, the magnetic transition temperatures are rather low ($T_{C,Ferri}<\sim 25$ K, $T_N<\sim 18$ K) and for further studies of this phase it will be essential to go substantially below the 8/10 K limit set by the present experimental equipment. Moreover, it should also be put efforts into improvement of the sample quality by systematic optimization of the synthesis and annealing procedures. With access to such better means for the experimental exploration it is highly appropriate to re-examine the crystal and magnetic structures in the ferri- and antiferromagnetic states of $Ca_3Co1_{1-v}Mn_vCo2O_6$. The magnetic phase diagram also needs closer attention and here many more samples with better composition resolution is required.

Acknowledgment

This work has received support from the Research Council of Norway, Grant 15818/S10 (NANOMAT).

References

[1] R. Vidya, P. Ravindran, H. Fjellvåg, A. Kjekshus, O. Eriksson, Phys. Rev. Lett. 91 (2003) 186404.
[2] M.-H. Whangbo, D. Dai, H.-J. Koo, S. Jobic, Solid State Commun. 125 (2003) 413.
[3] R. Frésard, C. Laschinger, T. Kopp, V. Eyert, Phys. Rev. B 69 (2004) 140405.
[4] V. Eyert, C. Laschinger, T. Koop, R. Frésard, Chem. Phys. Lett. 385 (2004) 249.
[5] A. Maignan, V. Hardy, S. Hébert, M. Drillon, M.R. Lees, O. Petrenko, D.M.K. Paul, D. Khomskii, J. Mater. Chem. 14 (2004) 1231.
[6] E.V. Sampathkumaran, N. Fujiwara, S. Rayaprol, P.K. Madhu, Y. Uwatoko, Phys. Rev. B 70 (2004) 014437.
[7] E.V. Sampathkumaran, Z. Hiroi, S. Rayaprol, Y. Uwatoko, J. Magn. Magn. Mater. 284 (2004) L7.
[8] A. Villesuzanne, M.-H. Whangbo, Inorg. Chem. 44 (2005) 6339.
[9] H. Wu, M.W. Harerkort, Z. Hu, D.I. Khomskii, L.H. Tjeng, Phys. Rev. Lett. 95 (2005) 186401.
[10] D. Dai, M.-H. Whangbo, Inorg. Chem. 44 (2005) 4407.
[11] K. Takubo, T. Mizokawa, S. Hirata, J.-Y. Son, A. Fujimori, D. Topwal, D.D. Sarma, S. Rayaprol, E.V. Sampathkumaran, Phys. Rev. B 71 (2005) 073406.
[12] T. Burnus, Z. Hu, M.W. Haverkort, J.C. Cezar, D. Flahaut, V. Hardy, A. Maignan, N.B. Brookes, A. Tanaka, H.H. Hsieh, H.-J. Lin, C.T. Chen, L.H. Tjeng, Phys. Rev. B 74 (2006) 245111.
[13] C.H. Hervoches, H. Fjellvåg, A. Kjekshus, V.M. Fredenborg, B.C. Hauback, J. Solid State Chem. 180 (2007) 628.
[14] C.H. Hervoches, V.M. Fredenborg, A. Kjekshus, H. Fjellvåg, B.C. Hauback, J. Solid State Chem. 180 (2007) 834.
[15] D. Flahaut, A. Maignan, S. Hébert, C. Martin, R. Retoux, V. Hardy, Phys. Rev. B. 70 (2004) 094418.
[16] G.V. Bazuev, V.G. Zubkov, I.F. Berger, V.N. Krasil'nikov, Russ. J. Inorg. Chem. 46 (2001) 317;
V.G. Zubkov, G.V. Bazuev, A.P. Tyutyunnik, I.F. Berger, J. Solid State Chem. 160 (2001) 293.
[17] S. Rayaprol, K. Sengupta, E.V. Sampathkumaran, Solid State Commun. 128 (2003) 79.
[18] Y.J. Choi, H.T. Yi, S. Lee, Q. Huang, V. Kiryukhin, S.-W. Cheong, Phys. Rev. Lett. 100 (2008) 047601.
[19] S. Niitaka, H. Kageyama, M. Kato, K. Yoshimura, K. Kosuge, J. Solid State Chem. 146 (1999) 137.
[20] A. Maignan, S. Hébert, C. Martin, D. Flahaut, Mater. Sci. Eng. B–Solid State Mater. Adv. Technol. 104 (2003) 121.
[21] N. Mohapatra, E.V. Sampathkumaran, Solid State Commun. 143 (2007) 149.
[22] H. Wu, Z. Hu, D.I. Khomaskii, L.H. Tjeng, Phys. Rev. B 75 (2007) 245118.
[23] T. Burnus, Z. Hu, H. Wu, J.C. Cezar, S. Niitaka, H. Takagi, C.F. Chang, N.B. Brookes, H.-J. Lin, L.Y. Jang, A. Tanaka, K.S. Liang, C.T. Chen, L.H. Tjeng, Phys. Rev. B 77 (2008) 205111.
[24] H. Fjellvåg, E. Gulbrandsen, S. Aasland, A. Olsen, B.C. Hauback, J. Solid State Chem. 124 (1996) 190.
[25] S. Aasland, H. Fjellvåg, B. Hauback, Solid State Commun. 101 (1997) 187.
[26] B.C. Hauback, H. Fjellvåg, O. Steinsvoll, K. Johansson, O.T. Buset, J. Jørgensen, J. Neutron Res. 8 (2000) 215.
[27] J. Rodríguez-Carvajal, Physica B 192 (1993) 55.
[28] L. Pauling, The Nature of the Chemical Bond, third ed., Cornell University Press, Ithaca, 1960.
[29] J.S. Smart, Effective Field Theories of Magnetism, Saunders, Philadelphia, 1966.